AGU PUBLICATIONS

Radio Science

RESEARCH ARTICLE
10.1002/2014RS005409

Special Section:
Beacon Satellite Symposium 2013

Predictions of HF system performance for propagation through disturbed ionospheres measured using low-Earth-orbit satellite radio beacon tomography

Paul A. Bernhardt[1], Matthew A. Hei[2], Carl L. Siefring[1], and Matthew R. Wilkens[2]

[1]Plasma Physics Division, Naval Research Laboratory, Washington, DC, USA, [2]Sotera Defense, Herndon, Virginia, USA

Key Points:
- Radio beacon tomography
- HF ray tracing through the reconstructions
- Experimental verification

Correspondence to:
P. A. Bernhardt,
Paul.Bernhardt@nrl.navy.mil

Citation:
Bernhardt, P. A., M. A. Hei, C. L. Siefring, and M. R. Wilkens (2014), Predictions of HF system performance for propagation through disturbed ionospheres measured using low-Earth-orbit satellite radio beacon tomography, *Radio Sci.*, *49*, 506–517, doi:10.1002/2014RS005409.

Received 2 MAR 2014
Accepted 26 JUN 2014
Accepted article online 1 JUL 2014
Published online 17 JUL 2014

Abstract The CERTO radio beacon on the C/NOFS satellite sends VHF/UHF radio signals at 150 and 400 MHz to provide measurements of integrated electron density or Total Electron Content (TEC) by an east-west chain of ground receivers in Peru. Computerized Ionospheric Tomography (CIT) is used to convert the TEC data into two-dimensional images of electron densities with maximum 5×5 km resolution in Longitude-Altitude space. These images are updated every 95 min as the C/NOFS satellite passes over the receiver network in its low-latitude orbit with an inclination of 12°. The 2-D, high-resolution images of the ionosphere are used to predict the impact of equatorial plasma structures on HF propagation of radar and radio signals. Electron density measurements from the NRL radio tomography chain across Peru are used for simulations of the performance by HF one-way links. HF rays from transmitter to receiver are traced through the electron density images produced by radio beacon tomography. Eight separate paths are found between a transmitter and ground receiver separated by 2000 km. A total of 36 backscatter echoes are found with unique group delay, Doppler frequency shift, phase delay, and echo amplitude. This multipath effect explains the range and Doppler spreading of observations for HF monostatic radar propagation through *F* layer irregularities. This type of analysis is useful for prediction and interpretation of range and Doppler observations from HF systems including over-the-horizon and SuperDARN radars, HF Geolocation Arrays, and HF communications networks.

1. Introduction

The effectiveness of long-range HF radars, geolocation, and communications systems is influenced by the plasma structures in the ionosphere. Over-the-horizon (OTH) and SuperDARN radars detect ground scatter and plasma irregularity echoes using HF waves that have been bent or refracted around the earth by the *F* layer ionosphere. The accuracy of HF radar scatter location estimation is dependent on the accuracy in the knowledge of the intervening ionosphere. For a relatively undisturbed ionosphere with uniform horizontal density gradients, the technique of oblique ionograms may used to provide this electron density knowledge and HF ray tracing is used to estimate the propagation delays and raypath bending between the transmitter and long-range target.

The two major types of HF radars are (1) over the horizon (OTH) and (2) SuperDARN. The OTH radar tracks the locations of near earth targets such as ships and aircraft using a sky wave mode that relies on ionospheric refraction [*Headrick*, 1990]. OTH radars measure the group range and Doppler frequency shift caused by scatter from the target. The SuperDARN radar systems track auroral plasma irregularities that move in the convection electric fields at high latitudes [*Greenwald et al.*, 1995]. The SuperDARN radar "target" is the field aligned irregularity (FAI) structures driven by electron precipitation currents associated with the aurora. Even though this target is in the ionosphere, the HF rays to the scatter point are determined by the horizontal and vertical electron density gradients between the ground radar and the FAI target region. Satellite-based measurements of the electron density volume through which the HF rays propagate can greatly improve the accuracy of the HF scatter point location especially if the propagation medium is highly structured.

HF geolocation systems become less effective at determining a source position for propagation through plasma irregularities on the bottomside ionosphere. HF multipath arises for long-distance propagation from a single transmitter in a structured ionosphere. This is responsible for received rays with multiple elevation

angles. These multiple angles of arrival at an HF geolocation site will complicate the analysis to estimate a single transmitter location. Attempts to compute ray trajectories back to a transmitter location require an accurate description of the electron density structures in the region between the transmitter and receiver locations.

Satellite beacon transmissions to a linear chain of ground receivers can provide total electron (TEC) data along multiple paths in the 2-D plane that contain the HF ray trajectories between transmitter and receiver. With a dense array of ground receivers, the TEC data may be processed tomographically to yield electron density maps with enough accuracy to reliably predict HF ray trajectories.

2. HF Propagation Modes in a Structured Ionosphere

The spatial resolution requirements for radio propagation through a highly resolved ionosphere are briefly described. HF Propagation in the ionosphere is affected by scatter, diffraction, and refraction from plasma structures depending on the scale sizes of the irregularities. The processes for electromagnetic waves in the ionosphere are described by solutions of Maxwell's Equations including the absorptive effects of electron-neutral collisions and the birefringence effects of the earth's magnetic field [*Yeh and Liu*, 1972].

Scattering of electromagnetic waves by plasma field aligned irregularities (FAI) is an important source of clutter for HF radars. The scattering cross section from FAI has been derived by *Simonich and Yeh* [1972] and *Yeh and Liu* [1972] to describe cross-mode and self-mode scattering for the characteristic ordinary and extraordinary modes in the ionosphere. The maximum scattering occurs for a wave normal vector in the mirror direction relative to the incident wave normal. Prediction of backscatter in a measured ionosphere requires knowledge of the electron densities with wavelength resolution better than one half the EM wavelength in the medium. At HF (3 to 30 MHz), this backscatter irregularity scale is 5 to 50 m. Whereas large region (thousands of km) estimation of electron densities with 5 km spatial resolution is feasible with low Earth orbit (LEO) satellite radio beacon tomography [*Hei et al.*, 2014], reliable estimates with better than 50 m accuracy is not possible over the areas of propagation for long-range HF signals.

Diffraction of an EM wave can be considered as continuous forward scattering through the refractive index structures in the plasma. The phase front for a wave is corrugated by phase enhancements introduced by the electron density irregularities. For an ionosphere model to be sufficiently accurate to predict the effects of diffraction, the spatial resolution in the model must be less than the Fresnel diffraction scale $d_F = (\lambda D)^{1/2}$ [*Rino*, 2011]. For HF waves in the 3 to 30 MHz frequency range ($\lambda = 100$ to 10 m wavelength range) propagating over distances of D = 2000 km, the Fresnel diffraction scale ranges from 10 to 3 km so the ionospheric spatial resolution should be about 1 km or less. Radio beacon tomography with 5 km spatial resolution is not able to provide the resolution needed for computing diffraction effects on the waves.

If the diffraction effects can be neglected, then the propagation is governed by the fundamental equations of geometric optics. In an isotopic medium, the ray trajectories are determined only by a scalar refractive index that is independent of propagation direction. In an anisotropic medium, refractive index for the ray trajectories are dependent on both direction of the wavenormal vector and the spatial position in the medium. The ray tracing equations for propagation in a magnetized plasma is derived from Maxwell's equations assuming that the free space wavelength goes to zero [*Yeh and Liu*, 1972]. Ray trajectories are computed starting from a point $\mathbf{r} = \{x, y, z\}$ with an initial wavenormal direction vector $\mathbf{n} = \{n_x, n_y, n_z\}$ normalized so $|\mathbf{n}|$ = refractive index n. The propagation medium is defined in terms of a refractive index Hamiltonian such as

$$H(\mathbf{r}, \mathbf{n}, t) = \frac{\left(n_x^2 + n_y^2 + n_y^2\right)^{1/2}}{n(\mathbf{r}, \mathbf{n}, t)} - 1 \equiv 0 \tag{1}$$

where $n(x, y, z, n_x, n_y, n_z)$ is derived from the Appleton-Hartree, Sen-Wyller, Booker Quartic, or another formulation for the refractive index in a magnetoionic medium [*Yeh and Liu*, 1972; *Jones and Stephenson*, 1975; *Budden*, 1985]. The raytrace equations are

$$\frac{d\mathbf{r}}{d\tau} = \frac{c}{\omega} \nabla_n H(\mathbf{r}, \mathbf{n}, t) \text{ and } \frac{d\mathbf{n}}{d\tau} = -\frac{c}{\omega} \nabla_n H(\mathbf{r}, \mathbf{n}, t) \tag{2}$$

where τ is the group delay along the raypath. The time dependence (t) in these equations is needed if the ionospheric plasma is not in steady state. An evolving ionosphere leads to Doppler shifts in the transmitted frequency at the receiver given by

$$\frac{d\omega}{d\tau} = \frac{c}{\omega}\frac{\partial H(\mathbf{r}, \mathbf{n}, t)}{\partial t} \tag{3}$$

The group path along the ray trajectory is the product of the speed of light and the group delay (i.e., $P' = c\tau$). In a plasma, the group path is greater than or equal to the physical path (s) and the phase path (P) computed with

$$\frac{ds}{d\tau} = \left|\frac{d\mathbf{r}}{d\tau}\right| \text{ and } \frac{dP}{d\tau} = \mathbf{n} \cdot \frac{d\mathbf{r}}{d\tau} \tag{4}$$

Finally, the amplitude variation along the ray trajectories is computed from the spreading or convergence of the cross-sectional area for a tube of rays propagated to the same group path [*Yeh and Liu*, 1972; *Budden*, 1985; *Nickisch*, 1988].

The two ordinary and extraordinary (O-Mode and X-Mode) solutions to the refractive index and the two direction solutions (forward and reverse) yield four ray solutions from a given point at a given launch direction. For HF propagation from the ground, the characteristic polarization of O-Mode or X-Mode is initiated with a polarization that excites that specified mode when the ray enters the ionosphere. If the ray is refracted back to the ground by the plasma, it arrives with the same characteristic polarization.

In a model ionosphere with structure scales larger than a Fresnel scale, geometric ray tracing and associated quantities integrated along the raypaths can be used to predict many of measureable performance parameters of an HF radar system. Tomographically determined electron densities for radio beacon satellites in low Earth orbit are given in the next section. Ray tracing through these density estimations provide predictions for HF system parameters including group delay, Doppler shifts, phase delay, geometric path length, and received signal amplitude.

3. High-Resolution Imaging of Equatorial Ionospheric Irregularities Using Radio Beacon Tomography

For prediction of HF propagation through a structured ionosphere, the electron densities must be specified in the propagation volume with the highest possible resolution. Radio and ultraviolet measurement techniques, either individually or separately, can be used to provide satellite based observations of ionospheric electron density [*Bernhardt et al.*, 1998]. *Comberiate and Paxton* [2010] describe purely space-based observations of equatorial plasma bubbles with far ultraviolet (FUV) imaging that has the advantage of not depending on any ground instrumentation. The spatial resolution of the FUV technique using the SSUSI and GUVI instruments is about 20 km vertically and 160 km in the horizontal direction [*Comberiate and Paxton*, 2010].

GPS receivers in low Earth orbit (LEO) recording total electron content (TEC) employ L-Band transmissions from GPS satellites in medium Earth orbit (MEO). GPS occultation imaging of electron densities has been described by *Mitchell* [2003], *Angling and Cannon* [2004], *Jakowski et al.* [2006], *Anthes et al.* [2008], etc. to yield vertical resolution as good as 5 km but horizontal resolutions larger than 200 km. The GPS occultation technique relies on the presence of a GPS satellite close to the orbit plane of the LEO satellite with a GPS occultation receiver. *McNamara et al*. [2013] employ assimilate ionosonde profiles and GPS TEC data to determine bottomside electron densities.

As pointed out by *Bernhardt et al*. [1998], *Kamalabadi et al.* [2002], *Bernhardt and Siefring* [2006], and *Comberiate and Paxton* [2010], the highest resolution space-based imaging of electron densities in the ionosphere uses TEC from radio beacons in low Earth orbit transmitting to ground receiver chains. The resolution of the radio tomographic imaging is limited by the Fresnel zone to about 1 km in the horizontal and vertical directions. The actual spatial resolution is determined by the density of ground beacon receivers along the direction of the satellite orbit. Compensation for motion of the ionosphere during the time of satellite beacon pass can be accomplished by moving the beacon receivers in a reference frame of a stationary ionosphere. Evolution of the ionosphere during the satellite pass cannot be removed from the tomographic image.

A technique for reconstruction of a large region of the *F* layer ionosphere by combining wide sweep backscatter ionogram (WSBI) and quasi vertical incidence (QVI) data from OTH radars with LEO beacon TEC

data to a distribution of ground beacon receivers has been developed by *Fridman and Nickisch* [2001]. Their reconstruction program has produced electron density maps in the 3-D volume illuminated by the OTH radar covering 70° in azimuth and 3300 km in range using seven beacon receivers recording TEC from the TRANSIT satellites. This work provided greatly improved accuracies on the estimations of critical frequency (f_oF_2) and critical height (HMax) over the large 3-D volume illuminated by an OTH radar.

Placing all the measurements and reconstruction in a two-dimensional region rather than a three-dimensional volume should improve the resolution of the electron density specifications in that restricted geometry. The work described here combines the LEO beacon tomography with in situ and ionosonde data to provide a higher resolution description of the ionosphere in a 2-D vertical plane that can be used to predict HF radar performance in disturbed or structured regions of the ionosphere. For a highly structured ionosphere, multiple propagation paths exist between transmitter and target. Supplemental information provided by radio beacon tomography is needed to fully explain the OTH radar observations.

Ionospheric tilts in the meridian direction normal to the tomographic reconstruction plane are not measured by the satellite beacon technique. For East-West propagation, North-South gradients in ionosphere primarily affects the apparent azimuth of a radar target or geolocation source from ray bending out of the vertical plane in the zonal direction. By making the assumption of no gradients perpendicular to the 2-D image plane, the investigation focusses on in-plane propagation affects that affect the range and Doppler shifts in the HF signals at the expense of ignoring out of plane effects such as azimuthal determination errors. This assumption is most justified near the magnetic equator where plasma structures are most easily smoothed out by horizontal diffusion along magnetic field lines. At the equator, the plasma density gradients are much stronger in the vertical and zonal directions than in the meridional direction.

With the 2-D approximation for long-range propagation over a few thousand kilometers, the deviation of HF ray trajectories out of the horizontal-vertical propagation plane containing the ground transmitter and receiver is typically less than 0.1%. Consequently, a 2-D tomographic image of the electron densities in the propagation plane gives enough information to compute those effects of the ionosphere on the HF system performance near the equator associated with multiple paths set up by reflections from large-scale field aligned irregularities and bubbles. Reducing the ionospheric specification to a two-dimensional geometry allows imposing the highest resolution specifications on the plasma densities to the propagation region of interest.

Reconstruction of the equatorial *F* region using low-Earth-orbit (LEO) radio beacon tomography (LRBT) has been demonstrated using the Air Force C/NOFS satellite which has an orbital inclination of 12° [*Hei et al.*, 2014]. The CERTO beacon on C/NOFS continuously radiates VHF (150.012 MHz) and UHF (400.032 MHz) to ground beacon receivers near the equator around the world. Currently, the CERTO beacon signals are received in South America, middle Pacific Ocean, and Southeast Asia. The CERTO beacon is operated continuously throughout the C/NOFS orbit with some turn-offs when the satellite power becomes too low.

The NRL Coherent Electromagnetic Radio Tomography (CERTO) instrument on C/NOFS routinely transmits to an East-West chain of ground receivers across Peru as illustrated in Figure 1. The stations are located with a total distance of 840 km over the ground. The distance between neighboring sites range between 163 and 290 km. The C/NOFS satellite is in an elliptical orbit with altitudes ranging from 400 to 800 km altitude. The projected spacing between the beacon-to-receiver paths in the ionosphere is on the order of 50 km in the ionosphere at 350 km altitude. This high density of integration paths in the ionosphere permits 5 km resolution of electron densities to be recovered by computerized ionospheric tomography [*Hei et al.,* 2014].

The two-dimensional imaging is limited by a number of factors including (1) physical displacement of the receivers away from a line parallel to the satellite orbit and (2) ionospheric tilts in the meridional direction from large-scale gradients and traveling ionospheric disturbances. The current tomography array is linear with stations chosen based on location of power and internet connectivity. Establishment of parallel receiver chains to the north and south of the current array (Figure 2) would allow estimation of the horizontal tilts normal to the existing reconstruction plane. The assumption of uniformity of the ionosphere in the north-south direction has not been tested with measurements. This paper only demonstrates the utility of radio beacon tomography near the equator when there are no meridional gradients the *F* layer.

Figure 1. Trajectory of the C/NOFS satellite relative to the five station tomography receiver chain in Peru. The CERTO beacon on C/NOFS transmits 150 and 400 MHz to the ground receivers for measurements of relative total electron content (RTEC) between the satellite and receiver. These TEC data are augmented with in situ electron density measurements on the satellite and ground ionosonde data to yield 2-D images of electron density.

An east-west chain of ground receivers and the satellite orbit defines the reconstruction plane for the tomographic imaging (Figure 2). The tomographic processing for electron densities near the equator take advantage of several factors including the followig: (1) the electron density gradients are small along the north-south magnetic field lines, (2) the in situ electron density at the C/NOFS PLP instrument provides a boundary condition at the top of the electron density image, (3) the digisonde at Jicamarca Peru gives a good initial guess for the plasma density profile of the bottom of the ionosphere, (4) the satellite orbit moves at about 7.7 km/s so the electron densities can be treated as stationary during the beacon overflight, and, most import, (5) the orbit period of the satellite is 95 min so an update of the electron densities are available 16 times per day.

The Multiplicative Algebraic Reconstruction Technique (MART) provides an electron density map and absolute TEC that is consistent with the observations. Details on this procedure are given in a number a papers including *Kersley et al.* [1997], *Pryse et al.* [1998], *Bernhardt et al.* [1998], *Kunitsyn and Tereshchenko* [2003], *Bernhardt and Siefring* [2006], and *Hei et al.* [2014].

To demonstrate the utility of high-resolution radio beacon tomography for prediction of HF propagation effects, three successive sets of TEC data were processed using the MART algorithm and the C/NOFS CERTO observations of TEC recorded by the NRL receiver chain in Peru. Examples of the reconstructed electron densities are shown in Figure 3. Three successive passes on 02 February 2010 were chosen because they had the largest simultaneous TEC variability at the four sites at the Peruvian cities of Huancayo (−75.22°E , −12.00°N), Ayacucho (−74.20°E, −12.03°N), Cusco (−71.97°E, −13.53°N), and Puerto Maldonado (−69.18°E, −12.58°N). After the electron densities were estimated in the 2-D plane of the C/NOFS orbit and ground receiver chain, integration through these densities was used to recover the TEC measurements. The difference error in the absolute TEC was less than 9% for all of the examples. The horizontal and vertical resolution is 5 x 5 km, respectively, at the center of the image and 20 x 5 km at the edges [*Hei et al.*, 2014].

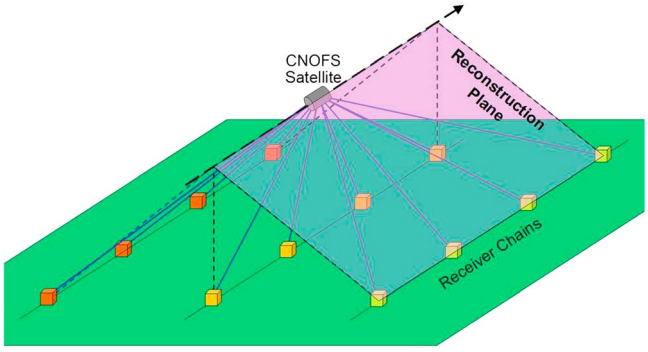

Figure 2. Oblique planes for imaging of electron densities using computerized ionospheric tomography with low-Earth-orbit beacons moving parallel to a line of ground receivers. The beacon signals from the C/NOFS CERTO transmitter are received around the world from receivers as far as 1000 km to the north or south of the low inclination (12°) of the satellite.

The plasma densities are evolving in time by (1) decay, (2) horizontal motion, (3) vertical drifts, and (4) photoionization after local sunrise at altitude in the ionosphere. The successive electron density maps in Figure 3 provide a history of the decay of plasma structures after midnight

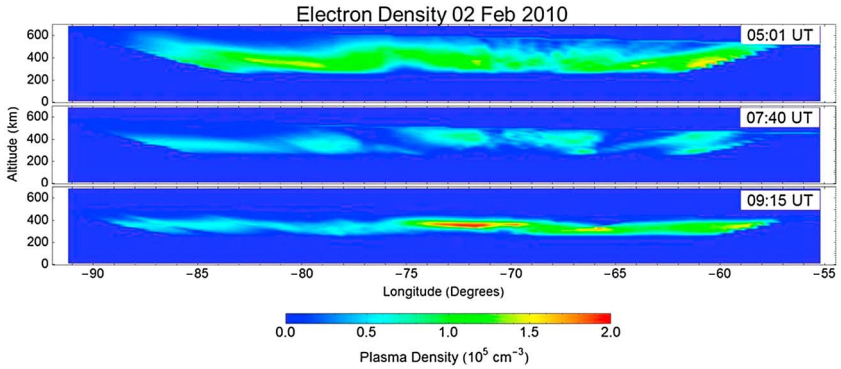

Figure 3. Electron density contours of the equatorial ionosphere obtained by analysis of C/NOFS TEC observations with computerized tomography. Each image is composed of 81 by 51 pixels in a two-dimensional (zonal and vertical) plane.

before sunrise. The electron density snapshots are displayed every 95 min which is the C/NOFS orbit period. The tomographic imaging has been used to determine the structures at late time for comparison with in situ sensors on C/NOFS and with observations of the Jicamarca ground radar [*Hei et al.*, 2014]. The in situ sensors of electron densities and plasma drifts provide only local observations at the satellite. The tomographic images are used to provide a large area context for the in situ data. In particular, the C/NOFS in situ observations have widely varying interpretations depending if the satellite is flying above, though, or even below the bulk of the ionospheric plasma. The horizontal motion of the plasma irregularities is determined from the electron density observations in Figure 3. The peak in the cross correlation between the image at 05:10 UT and at 07:40 UT provides an estimate of zonal (east-west) plasma drift of −27 m/s. This value is in agreement with the in situ plasma drift measurements obtained with the CINDI instruments on C/NOFS. The Jicamarca radar operation at 05:01 UT yields vertical drifts of 20 m/s downward.

Radio beacon tomography yields electron density maps with higher resolution than any other techniques over large ground ranges. Linear arrays of ground ionosondes, spatial scans with incoherent scatter radars, arrays of GPS receivers, FUV scans from satellites in LEO, or GPS occultation maps cannot by themselves provide the high-resolution electron density data shown in Figure 3. The radio beacon tomography maps are well suited for predictions of ionospheric effects on HF systems. The quasi-periodic plasma clumping of the electron densities as well as the motion of the irregularities will produce observable effects on HF radar ray trajectories. Computations of these effects of the structured ionosphere are illustrated in the next section.

4. Predictions of Long-Range Propagation for HF Signals

HF communications and radar system performance requires selection of the operating frequency for propagation through the ionosphere to the receiver or target location. Selection of HF OTH radar transmitter frequencies are often computed with real-time measurements of the range delays from ground echoes with wide band frequency sweeps. Frequency selection for shortwave communication and direction finding systems often relies on receiving of existing HF radio sources at large distances. Knowledge of the existing electron densities in the ionosphere coupled with HF ray tracing provides estimates of propagation conditions without these additional active HF sources.

An example of over-the-horizon (OTH) radar is used as an example of propagation prediction based on a high-resolution reconstructed ionosphere. The tomographic reconstructions of the electron densities at 05:10 UT in Figure 3 are used to define the HF ray trajectories from a ground transmitter located 1000 km from the center of the data set. The clumps of plasma reflect both O-Mode and X-Mode rays into crossing trajectories. The raypaths are computed using the raytrace equations defined in Section II-3 written in Cartesian coordinates and solved using Mathematica V9.0. The Appleton-Hartree formula for the refractive index is applied in free space ($n = 1$) and in regions where the refractive index is greater than one half. In dense regions of the plasma where the refractive index is less than one half and near wave reflection points, the Booker Quartic formula provides the refractive index. Initially the rays are computed starting with the local vertical direction (0° zenith angle) to nearly horizontal (88° zenith angle) with 0.5° steps in the zonal (west to east) direction. This same raytrace code with a low-frequency refractive index specification

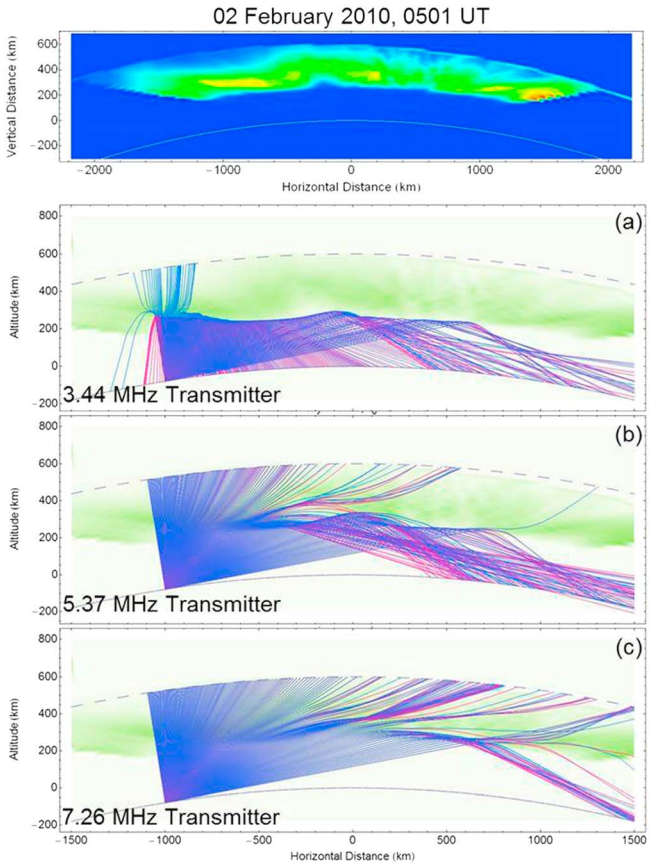

Figure 4. Multiple ray tracing to show long-distance propagation of HF signals in a structured ionosphere with transmitter frequencies chosen to be (a) 0.9, (b) 1.4, and (c) 1.9 the maximum critical frequency in the *F* layer. The O-Mode (blue) and X-Mode (red) paths illuminate portions of the earth with multiple crossed paths. The rays are terminated either at the earth's surface after reflection or at 600 km altitude after passing through the ionosphere.

has been used previously by *Bernhardt et al.* [2012] for propagation of MHD and Whistler mode waves in the ionosphere.

Sample ray trajectories at 0.9, 1.4, and 1.9 times the maximum plasma frequency in the ionosphere are shown in Figure 4. Except for the vertical raypaths, all of the transmissions at 3.44 MHz are refracted to the ground by the structured ionosphere (Figure 4a). The HF transmitter provides nonuniform illuminations on the ground at all ranges from the transmitter point to horizontal ranges greater than 2500 km. Irregular refraction in the structured ionosphere yields several rays to the same ground location resulting in multipath propagation for horizontal ranges above 1500 km from the HF source.

At 5.37 MHz, about 60% of the rays penetrate the ionosphere through the electron density structures. The other 40% of the 5.37 MHz rays are refracted by the irregularities to form a complex multipath pattern on the ground at horizontal distances 1500 to 2500 km from the transmission point. At the highest frequency (7.26 MHz), all but lowest elevation rays pass through the ionosphere. The only 7.26 MHz rays make it to the ground clump together into a multipath beam 2500 km from the transmitter.

Out of the manifold of ray trajectories launched from a ground transmitter, a homing algorithm is used to establish the links between two points on the ground separated over a long horizontal distance [*Strangeways*, 2000]. Homing is initiated by finding three rays from a ground transmitter site that form a triangle of intersection points on the earth that contains the desired reception location. Interpolation is used to estimate the next launch angles (elevation and azimuth) that produce a raypath closer to the desired target point. With this point, the interpolation provides a new estimate of the ray launch direction and the iteration continues.

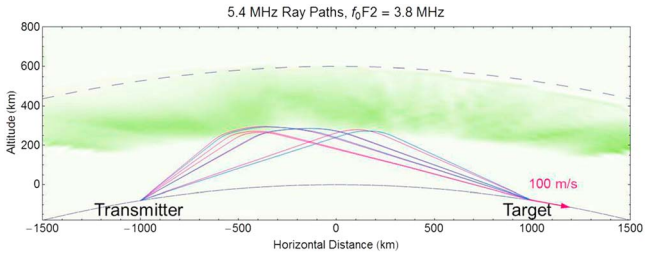

Figure 5. Computed raypaths linking two points by 5.37 MHz propagation though a structured ionosphere. Eight point-to-point paths are found using a ray tracing homing algorithm starting with the ray trajectories illustrated in Figure 4b. Note that the target point is moving along the earth's surface at 100 m/s.

Using raypath homing, eight different propagation paths where found between transmitter and target sites separated by 2000 km (Figure 5). The homed rays were traced in the reconstructed ionosphere at 05:10 UT on 10 February 2010. Six iterations of the ray tracing homing algorithm were required to provide propagation

Table 1. Computed One-Way Parameters for 5.37 MHz

Transmit Zenith Angle	Transmit Elevation	Received Zenith Angle	Received Elevation	Propagation Mode	Received Intensity	Group Path	Ionospheric Doppler	Target Doppler
59.73°	30.27°	81.44°	8.56°	Extraordinary	−16.62 dB	2126 km	0.283 Hz	−1.482 Hz
60.89°	29.11°	81.21°	8.79°	Ordinary	−4.42 dB	2128 km	0.282 Hz	−1.480 Hz
63.18°	26.82°	83.99°	6.01°	Extraordinary	−7.93 dB	2123 km	0.259 Hz	−1.515 Hz
65.97°	24.03°	84.22°	5.78°	Extraordinary	−5.64 dB	2124 km	0.251 Hz	−1.523 Hz
69.82°	20.18°	79.20°	10.80°	Ordinary	−8.32 dB	2131 km	0.278 Hz	−1.474 Hz
70.17°	19.83°	79.36°	10.64°	Extraordinary	−7.82 dB	2130 km	0.275 Hz	−1.478 Hz
79.88°	10.12°	75.51°	14.49°	Extraordinary	−3.83 dB	2116 km	0.268 Hz	−1.459 Hz
81.04°	8.96°	74.36°	15.64°	Ordinary	0.00 dB	2117 km	0.272 Hz	−1.446 Hz

paths that landed within one meter of the target point. Three O-Mode paths and five X-Mode paths are set up between the transmitter and target locations. In an unstructured ionosphere, one expects that only one O-Mode and one X-Mode raypath would be established between the two ground points.

The parameters for the eight propagation paths derived from the ray tracing computations are summarized in Table 1. These parameters can be observed with receiving systems located at the target end of the propagation path shown in Figure 5. All of the receiver azimuths are 270° because the electron densities are assumed to be aligned north-south with the earth's magnetic field lines. The received zenith (or elevation) angles are distributed in a more narrow range than the initial launch angles because six of the eight paths are produced by refractive mirroring from the electron density enhancements closer to the transmitter than the receiver/target point. An HF geolocation array measuring the received signal zenith angle would see the distribution of distribution angles given in Figure 6.

The target in Figure 5 is assumed to be moving to the right along the surface of the earth with a speed of 100 m/s. A receiver at the target location will see Doppler shifts in the transmitted signals from two sources. First, the ionosphere structures are moving with the measured drifts of 27 m/s to the left and are descending at a speed of 20 m/s. The ionospheric Doppler is computed with the formula

$$\frac{d\omega}{d\tau} = \frac{c}{\omega}\frac{\partial H(\mathbf{r},\mathbf{n},t)}{\partial t} = \frac{c}{\omega}\frac{\partial H(\mathbf{r},\mathbf{n},t)}{\partial n_e}\frac{\partial n_e(\mathbf{r},t)}{\partial t} = -\frac{c}{\omega}\frac{\partial H(\mathbf{r},\mathbf{n},t)}{\partial n_e}\,\mathbf{v}_e\cdot\nabla n_e(\mathbf{r}) \tag{5}$$

where $\mathbf{v}_e$ is the plasma drift velocity vector and the electron density is assumed frozen as it is transported by this velocity. The dropping of the layer is the primary source for the ionospheric Doppler shifts near 0.27 Hz given in Table 1. The target Doppler is computed using the target velocity vector projected along the propagation vector of each raypath. For a receiver located on the 100 m/s target, Doppler frequency shifts are on the order of −1.5 Hz. The total Doppler shift observed at the receiver is the sum of the ionspheric and target Doppler shifts.

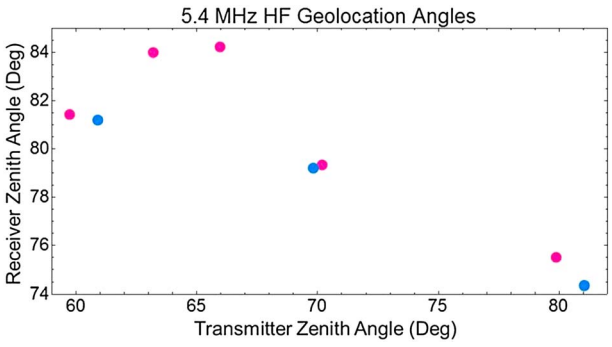

Figure 6. Computed zenith angles for O-Mode (Blue) and X-Mode (Red) rays propagating over the 2000 km horizontal distance between ground emitter and ground detector. The ionosphere supports more X-Mode paths than O-Mode paths because the X-Mode is more strongly refracted at lower densities.

The time delay along each raypath is multiplied times the speed of light to give the group path length given in Table 1. The spreading of rays launched by small amounts (±0.01° in elevation) from the homed rays provides a measure of the signal intensity at the receiver. These one-way intensities are express in decibel relative to the strongest path in Table 1. Combining the Doppler, group path and intensity computations yields the Doppler Range Intensity map given in Figure 7. This DRI display is representative for multipath HF propagation through a structured ionosphere.

Quasi-monostatic HF radar systems such as OTH and SuperDARN Radars have

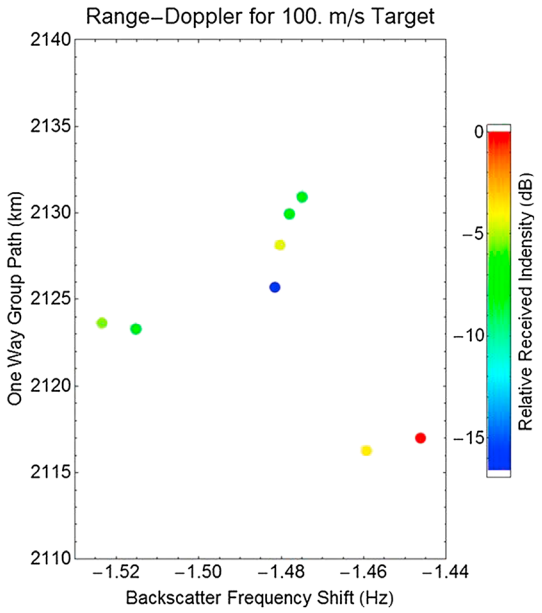

Figure 7. Doppler Range Intensity (DRI) prediction for one-way propagation at 5.37 MHz to a ground receiver moving 100 m/s at a distance of 2000 km. The variations in the received signals are the result of waves traveling along eight separate paths in a moving, structured ionosphere.

receivers located near the transmitter points. Simulations of the target echoes for monostatic HF radars involves computations of the Doppler shifts, time delays, and signal amplitudes of the forward paths coupling into return paths along the same ray trajectories. Each of the eight paths illustrated in Figure 5 are reciprocal channels for return echoes [*Budden,* 1985]. The coupling between the forward and reverse propagation for a backscatter radar is illustrated in Figure 8. Eight round trip echoes are formed by target scatter into the same raypath. Handshaking between separate forward and reverse paths yields 28 roundtrip channels. The group path, Doppler shifts, and intensity in (dB) for a pair of paths are the sums of these quantities for each of the individual paths. Since coupling of path A into path B is identical to coupling of path B into path A, the intensity on the handshaking roundtrip channels is Path A Intensity (dB) + Path B Intensity (dB) + 3 (dB).

The computed DRI graph for the bistatic HF radar operating at 5.37 MHz is shown in Figure 9. The number of combination paths for scattering of n forward paths into the same return raypaths is $n(n+1)/2$. For the eight rays illustrated in Figure 5, a total of 36 target scatter points at the receiver. These points are spread by over 30 km in group range and by 0.15 Hz in frequency shift. The backscatter intensities from the target are computed with scattering assumed to be isotropic with equal excitation of ordinary and extraordinary modes. The relative scattered intensities have a range between −33.2 and 0 dB as indicated by the red-orange-yellow-green-blue scale of dots in Figure 9.

Next, consider the predictions of HF signal intensities in space. HF waves with frequencies substantially larger than the *E* or *F* layer critical frequencies may pass through the ionosphere along the refracted paths as illustrated in Figure 4. The electron density structures in the ionosphere focus and defocus these HF signals that can be observed on satellite receivers. The electron density images that are produced using radio tomography with VHF and UHF satellite beacon signals may be validated by measuring the HF signal strength with an HF digital receiver on the same satellite.

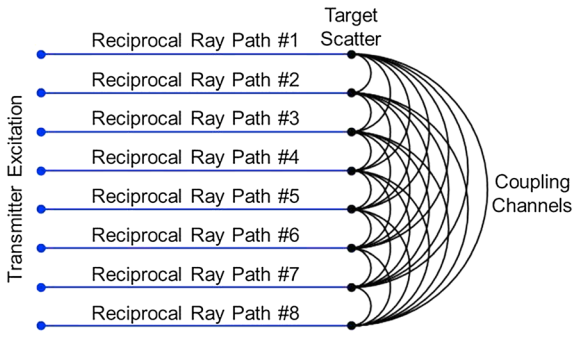

Figure 8. Multiple echo generation by multipath coupling of HF backscatter from a target. Target scatter is assumed to be isotropic and evenly divided between the O-Mode and X-Mode polarizations.

The 5.37 MHz raypaths that penetrate the ionosphere to 600 km altitude are used to compute the HF wave intensity in space. The spreading or clumping of the rays are proportional to the reduction and increase in wave intensity. Figure 10 illustrates this variation in signal strength along a satellite orbit indicated by the dashed line in Figure 4b. The signal intensity is normalized to unity for vertical rays from the transmitter. An isotropic antenna pattern is assumed for the ground HF system. Each of the computed peaks in wave intensity corresponds to a larger density in raypaths shown in Figure 4b. These wave focusing regions map back along the ray trajectories of regions of enhanced electron densities provided by the tomographic

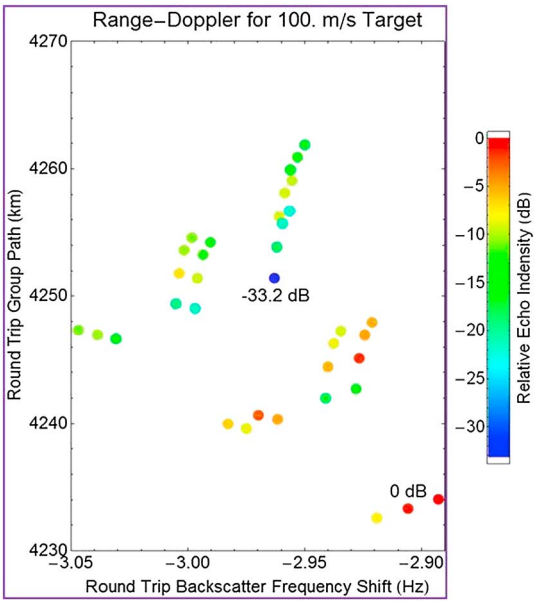

Figure 9. Spread in Doppler shifts and group path delays for the 36 echoes received with a backscatter HF radar from the moving target shown in Figure 5. The strengths of the echo intensities are indicated by the color of the points.

reconstructions at 05:10 UT in Figure 3. The average drop in signal strength with horizontal distance in Figure 10 is attributed to the increase in range as the satellite passes away from closest point of approach to the transmitter.

5. Conclusions

High-frequency (HF) propagation in a structured ionosphere produces complications in analysis and performance of radar, geolocation, and communications systems. The addition of radio beacon tomography using LEO beacons and chains of ground receivers supplemented with ionosonde or in situ electron density data greatly improves the ability to interpret the observations and capabilities of an HF instrument.

Tomographic images of post-midnight structures in the equatorial ionosphere have been used to predict the propagation of HF rays over long distances. The wave propagation simulations in the measured electron density structures have demonstrated range and Doppler spreading of the signal for one-way oblique paths and for backscatter to the transmitter. With a multipath environment supporting eight ground to ground modes, a total of 36 delayed echoes will be scattered to the transmission point with over 30 dB range in signal intensity.

The magnitudes of the high-latitude observations of both Doppler and Range spread at high latitudes are probably larger than the equatorial region predictions (Figures 7 and 9). Differences between plasma drift velocities and geometry of plasma irregularities in the two regions can partially explain these differences. Also, ray tracing computations have not included diffraction effects which can cause further frequency and range spreading of the received frequency dwells. The diffraction along a single raypath will introduce a spatial pattern in the HF wave amplitudes that will be recorded as temporal variations and frequency shifts. Future research should examine the feasibility of using tomographically resolved electron densities to predict this diffraction effect.

Future experiments near the equator may be conducted to replicate the predictions of Figures 6–11 by setting up an HF propagation link between the west and east borders of Peru. The in situ and radio beacon instruments on C/NOFS can periodically update the state of the ionosphere and the ground HF transmitter/receiver link can determine the effects of this ionosphere.

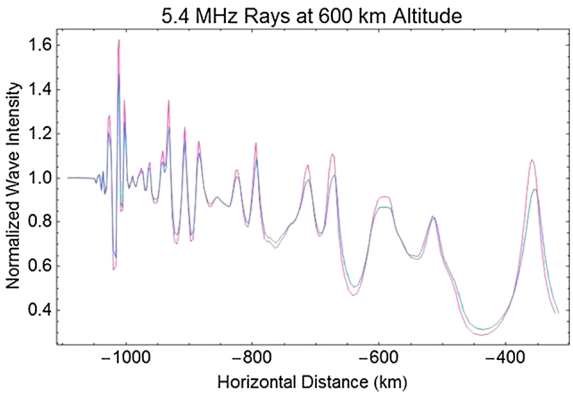

Figure 10. Predictions of HF wave intensity at 5.37 MHz measured with a satellite in low Earth orbit at 600 km altitude.

The accuracy and utility of radio beacon tomography for prediction of HF propagation can be validated using a LEO satellite that has both a dual frequency (CERTO) radio beacon and an HF receiver. Such satellite called ePOP/CASSIOPE was launched into an 80° inclination orbit by the Canadian Space Agency on 29 September 2013. The eight ePOP instruments are provided by scientists from Canada, Japan, and the United States. The CERTO beacon instrument on ePOP is similar to the one on C/NOFS that produced the tomographic images in this paper. The Radar Receiver Instrument (RRI) on ePOP has

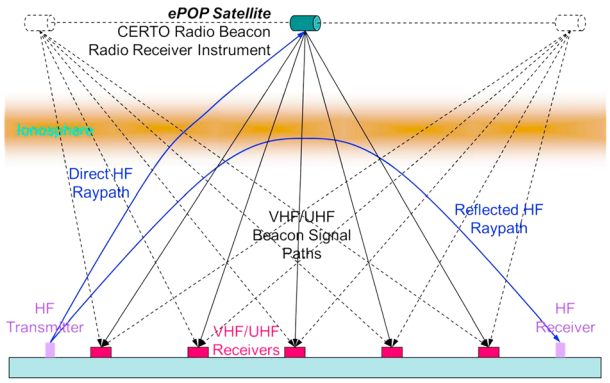

Figure 11. Diagram of high-latitude structure experiments using the CERTO radio beacon for ionospheric tomography and an HF propagation link. The radio receiver on ePOP can be added to yield space-based measurements of HF waves penetrating the ionosphere. The predictions of HF propagation based on radio beacon tomography can be validated with these experiments employing a full suite of radio, remote, and in situ instruments on C/NOFS, ePOP, or other satellites.

four 50 kHz channels that can record HF signal data at any frequency up to 30 MHz. The other instruments on ePOP provide in situ electron and ion distributions, GPS occultation measurements, optical imagery, neutral winds and density, and magnetic fields. With the ePOP or similar data, the type of predictions derived here for HF propagation in high-resolution images of the ionosphere can be tested. The plan for such experiments is illustrated in Figure 11.

In summary, quantitative predictions of HF propagation through a disturbed ionosphere may be produced using HF ray tracing through electron densities obtained at high resolution with radio beacon tomography from satellites in low Earth orbit. Future validation of this technique will use the ePOP/CASSIOPE satellite with a suite of eight instruments. For this study, the primary instruments will be the a multifrequency beacon and in situ plasma probes to provide the tomographic reconstruction data and the HF radio receiver instrument to validate estimates of the HF propagation to the satellite. The utility of this research is to identify ionospheric propagation effects that spread the HF signals in frequency, group delay, group phase, and intensity and to determine if radio beacon tomography can provide accurate enough electron density maps to predict these effects.

Acknowledgments

This research was supported by the NRL 6.1 Base Program. The operations of the C/NOFS satellite are provided by the Air Force Research Laboratory. The TEC data used in this paper are available from the first author by email request address Paul.Bernhardt@nrl.navy.mil.

References

Angling, M. J., and P. S. Cannon (2004), Assimilation of radio occultation measurements into background ionospheric models, *Radio Sci.*, *39*, RS1S08, doi:10.1029/2002RS002819.

Anthes, R. A., et al. (2008), The COSMIC/FORMOSAT-3 mission: Early results, *Bull. Am. Meteorol. Soc.*, *89*(3), 313–333.

Bernhardt, P. A., and C. L. Siefring (2006), New satellite based systems for ionospheric tomography and scintillation region imaging, *Radio Sci.*, *41*, RS5S23, doi:10.1029/2005RS003360.

Bernhardt, P. A., et al. (1998), Two-dimensional mapping of the plasma density in the upper atmosphere with computerized ionospheric tomography (CIT), *Phys. Plasmas*, *5*, 2010–2021.

Bernhardt, P. A., et al. (2012), Ground and space-based measurement of rocket engine burns in the ionosphere, *IEEE Trans. Plasma Sci.*, *40*, 1267–1285.

Budden, K. G. (1985), *The Propagation of Radio Waves*, Cambridge, England.

Comberiate, J., and L. J. Paxton (2010), Coordinated UV imaging of equatorial plasma bubbles using TIMED/GUVI and DMSP/SSUSI, *Space Weather*, *8*, S10002, doi:10.1029/2009SW000546.

Fridman, S. V., and L. J. Nickisch (2001), Generalization of ionospheric tomography on diverse data sources: Reconstruction of the three-dimensional ionosphere from simultaneous vertical ionograms, backscatter ionograms, and total electron content data, *Radio Sci.*, *36*, 1129–1139, doi:10.1029/1999RS002405.

Greenwald, R. A., et al. (1995), DARN/SuperDARN, *Space Sci. Rev.*, *71*(1–4), 761–796.

Headrick, J. H. (1990), *HF Over-the-Horizon Radar, Radar Handbook*, chap. 24, edited by M. Skolnik, McGraw Hill, Boston, Mass.

Hei, M. A., et al. (2014), Radio-tomographic images of post-midnight equatorial plasma depletions, *Geophys. Res. Lett.*, *41*, 13–19, doi:10.1002/2013GL056112.

Jakowski, N., C. Mayer, and V. Wilken (2006), GPS sounding of the ionosphere onboard CHAMP, in *Characterising the Ionosphere*, Meeting Proceedings RTO-MP-IST-056, Paper 26, pp. 26-1–26-16, RTO, Neuilly-sur-Seine, France.

Jones, R. M., and J. J. Stephenson (1975), A versatile three-dimensional ray Tracing computer program for radio waves in the ionosphere, U.S. Department of Commerce, *OT Report 75-76*.

Kamalabadi, F., et al. (2002), Tomographic studies of aeronomic phenomena using radio and UV techniques, *J. Atmos. Sol. Terr. Phys.*, *64*, 1573–1580.

Kersley, L., S. E. Pryse, I. K. Walker, J. A. T. Heaton, C. N. Mitchel, M. J. Williams, and C. A. Willson (1997), Imaging of electron density troughs by tomographic techniques, *Radio Sci.*, *32*, 1607–1621, doi:10.1029/97RS00310.

Kunitsyn, V. E., and E. D. Tereshchenko (2003), *Ionospheric Tomography*, Springer-Verlag, Berlin.

McNamara, L. F., M. J. Angling, S. Elvidge, S. V. Fridman, M. A. Hausman, L. J. Nickisch, and L.-A. McKinnell (2013), Assimilation procedures for updating ionospheric profiles below the F2 peak, *Radio Sci.*, *48*, 143–157, doi:10.1002/rds.20020.

Mitchell, C. N. (2003), Combining radio occultation measurements with other instruments to map the ionospheric electron concentration, in *First CHAMP Mission Results for Gravity, Magnetic and Atmospheric Studies 2003*, pp. 491–499, Springer, New York.

Nickisch, L. J. (1988), Focusing in the stationary phase approximation, *Radio Sci.*, *23*, 171–182, doi:10.1029/RS023i002p00171.

Pryse, S. E., L. Kersley, C. N. Mitchell, P. S. J. Spencer, and M. J. Williams (1998), A comparison of reconstruction techniques used in ionospheric tomography, *Radio Sci.*, *33*, 1767–1779, doi:10.1029/98RS01613.

Rino, C. L. (2011), *The Theory of Scintillation With Applications in Remote Sensing*, IEEE Press, New York.

Simonich, D. M., and K. C. Yeh (1972), A theory of scattering form irregularities in a magneto-ionic medium, *Radio Sci.*, *7*, 291–299, doi:10.1029/RS007i002p00291.

Strangeways, H. J. (2000), Effect of horizontal gradients on ionospherically reflected or transionospheric paths using a precise homing-in method, *J. Atmos. Sol. Terr. Phys.*, *62*, 1361–1376.

Yeh, K. C., and C. H. Liu (1972), *Theory of Ionospheric Waves*, Academic Press, New York.